Electron spin filter and polarizer in a standing light wave

Ahrens Sven*
Beijing Computational Science Research Center, Zhongguancun Software Park II, No. 10 West Dongbeiwang Road, Haidian District, Beijing 100193, China
(Dated: October 24, 2016)

We demonstrate the theoretical feasibility of spin-dependent diffraction and spin-polarization of an electron in two counter-propagating, circular polarized laser beams in a relativistic quantum simulation. Our proposal realizes the Stern-Gerlach experiment for free electrons, by interaction with electro-magnetic fields only. The spin-dynamics appears in a two-photon process of the Kapitza-Dirac effect in the Bragg regime. We further discuss the spin properties of the diffraction process by studying an analytically approximated solution of the time-evolution matrix. A classification scheme in terms of unitary or non-unitary propagation matrices is used for establishing a generalized and spin-independent description of the spin properties of the diffraction process.

PACS numbers: 42.50.Ct, 03.75.-b, 41.75.Fr, 42.25.Ja
Keywords: Quantum mechanics, Relativistic wave equations, Matter waves, Electron beams, Polarization, X-ray lasers

arXiv:1604.06201v3 [quant-ph] 21 Oct 2016

I. INTRODUCTION

The particle spin is an intrinsic, non-classical angular momentum. Historically this quantum mechanical degree of freedom has been provisionally proposed for the consistent explanation of the atom angular momentum [1]. Evidence for the existence of spin has been given in the Stern-Gerlach experiment by deflection of neutral silver atoms in an inhomogeneous magnetic field [2]. For charged particles, like free electrons however, Pauli gave reasons in 1932 that one may not detect the electron's spin by applying external electric or magnetic fields. The argument was that the separation of electrons may be unfeasible due to a limitation of the simultaneous exact knowledge of position and momentum according to Heisenberg's uncertainty principle [1, 3]. This is opposed with the continuous Stern-Gerlach experiment by Dehmelt, which is able to implicitly infer the electron spin configuration by measuring the electron's cyclotron frequency in a Penning trap [4]. The idea of a more straight forward spin separation like in the Stern-Gerlach experiment has been raised by considerations on a "Microscopic Stern-Gerlach magnet" [5]. The setup of such a device has been inspired by the experimental realization of the Kapitza-Dirac effect [6], in which particles are diffracted by a standing wave of light [7]. In fact, theoretical calculations show that the electron spin can be altered in the Kapitza-Dirac effect in a spin-insensitive way [8–13], leaving the question of an explicit and spin-dependent sorting mechanism unanswered.

In this paper we theoretically discuss the spin separation and spin polarization of the electron spin in the Kapitza-Dirac effect by using circularly polarized, strong X-ray laser beams. We demonstrate the spin-dependent diffraction by explicitly altering the initial electron spin configuration. Furthermore we discuss a general characterization method for the diffraction process's spin properties which is spin-independent, ie. independent of the initial and final spin configuration of the electron.

We note, that a first spin sensitive setup for electron diffraction, based on grating elements which affect the particle's phase, has been discussed recently by McGregor, Bach and Batelaan [14]. Also, at the final stage of our research, a new theoretical study from Dellweg and Müller is presented which concludes spin separation and polarization in a bi-chromatic, interferometric setup of three successive laser pulses [15].

The article is organized as follows: In section II A we describe the laser field and in section II B we introduce the notion of relativistic quantum dynamics in momentum space. We present a full simulation of the equations of motion in II C with a Gaussian-shaped, temporal interaction of the electron with the laser field, and we point out spin-dependent diffraction and spin-polarization effects. In section III we adapt an approximative solution of the quantum dynamics [12] for a laser field which propagates along the z-axis. Section IV discusses the spin properties of the analytic solution by starting with general considerations on the degrees of freedoms of the 2×2 submatrix which is responsible for the propagation of the electron spin. We further approximate the solution for different time-scales, ie. at instant times in section IV A and after an eighth of the period $2\pi/\Omega_S$ in section IV B, where Ω_S is a characteristic frequency of spin effects. For the latter case we investigate the spin-dependent diffraction in section IV C and spin-polarization of the electron in section IV D by comparing the dynamics with the a more exact analytic solution in appendix B and the numerical simulation of the quantum dynamics. In section IV E we discuss the extremal cases of the spin-dependent diffraction. We conclude in section V with outlining the implications of the discussed spin-dynamics, relating the studied effect to other experimental considerations and opening new perspectives which are based on the effect.

* ahrens@csrc.ac.cn

II. SIMULATION OF RELATIVISTIC QUANTUM DYNAMICS

For the description of the process we solve the quantum dynamics of the single particle Dirac equation

$$i\hbar\dot{\Psi}(\boldsymbol{x},t) = \left[c\left(-i\hbar\boldsymbol{\nabla} - \frac{q}{c}\boldsymbol{A}(\boldsymbol{x},t)\right)\cdot\boldsymbol{\alpha} + mc^2\beta\right]\Psi(\boldsymbol{x},t)\,, \tag{1}$$

in momentum space by making use of a plane wave expansion of the wave function [8–11]. The constants in Eq. (1) are the reduced Planck constant $\hbar$, the electron restmass m and the vacuum speed of light c. The α_i of the vector $\boldsymbol{\alpha}$ and β are the Dirac matrices.

A. The external electro-magnetic field

We describe the vector field of two counter-propagating, circularly polarized laser beams by

$$\boldsymbol{A}(\boldsymbol{x},t) = 2Aw(t)\cos(kz)\left[-\sin(\omega t)\boldsymbol{e}_x + \cos(\omega t)\boldsymbol{e}_y\right]\,, \tag{2}$$

with wavenumber k and frequency $\omega = ck$. Eq. (2) is a solution of the Maxwell equations, provided that the envelope function $w(t)$ was constant. We model the temporal interaction of the electron with the laser beam in our numerical simulation by using the envelope function

$$w(t) = \sin^2\left(\frac{\pi t}{\tau}\right)\,, \tag{3}$$

in accordance with earlier studies [8–12, 16, 17]. The parameter τ is the time period of the interaction.

B. Equations of motion in momentum space

For the description of the relativistic wave function, we introduce the bi-spinors

$$u_n^{+,\alpha} = \sqrt{\frac{\mathcal{E}_n + mc^2}{2\mathcal{E}_n}}\begin{pmatrix}\chi^\alpha \\ \frac{nck\hbar\sigma_z}{\mathcal{E}_n+mc^2}\chi^\alpha\end{pmatrix} \tag{4a}$$

$$u_n^{-,\alpha} = \sqrt{\frac{\mathcal{E}_n + mc^2}{2\mathcal{E}_n}}\begin{pmatrix}-\frac{nck\hbar\sigma_z}{\mathcal{E}_n+mc^2}\chi^\alpha \\ \chi^\alpha\end{pmatrix}\,, \tag{4b}$$

and the solutions of the free Dirac equation [8, 9]

$$\psi_n^{\gamma,\alpha}(\boldsymbol{x}) = \sqrt{\frac{k}{2\pi}}u_n^{\gamma,\alpha}e^{inkz}\,. \tag{5}$$

Here, $\mathcal{E}_n$ is the relativistic energy momentum relation

$$\mathcal{E}_n = \sqrt{(mc^2)^2 + (nck\hbar)^2} \tag{6}$$

and σ_x, σ_y and σ_z are the three Pauli matrices. The two component objects $\chi^\uparrow = (1,0)^T$, $\chi^\downarrow = (0,1)^T$ form a basis in the spinor space of the Pauli equation. The functions (5) are simultaneous eigenfunctions of the momentum operator, the free Dirac Hamiltonian and of the Foldy-Wouthuysen spin operator [18]. Correspondingly, the quantum numbers of the eigenfunctions denote the momentum $nk\hbar$, the sign of the eigenenergy $\gamma \in \{+,-\}$ and the spin $\sigma \in \{\uparrow,\downarrow\}$.

The relativistic wavefunction of the electron

$$\Psi(\boldsymbol{x},t) = \sum_{\substack{n\in\mathbb{N},\\ \alpha\in\{\uparrow,\downarrow\}}} c_n^\alpha(t)\psi_n^{+,\alpha} + d_n^\alpha(t)\psi_n^{-,\alpha} \tag{7}$$

is expanded in terms of the described eigenfunctions, where the time-evolution of the expansion coefficients $c_n^\alpha(t)$ and $d_n^\alpha(t)$ is obtained by projecting the Dirac equation (1) at the plane waves (5). We obtain a system of differential equations

$$i\hbar\dot{c}_n^\alpha(t) = \mathcal{E}_n c_n^\alpha(t) + \sum_{\substack{n'\in\mathbb{N},\\ \beta\in\{\uparrow,\downarrow\}}}\Big[V_{n,n'}^{+,\alpha;+,\beta}(t)c_{n'}^\beta(t) + V_{n,n'}^{+,\alpha;-,\beta}(t)d_{n'}^\beta(t)\Big]\,, \tag{8a}$$

$$i\hbar\dot{d}_n^\alpha(t) = -\mathcal{E}_n d_n^\alpha(t) + \sum_{\substack{n'\in\mathbb{N},\\ \beta\in\{\uparrow,\downarrow\}}}\Big[V_{n,n'}^{-,\alpha;+,\beta}(t)c_{n'}^\beta(t) + V_{n,n'}^{-,\alpha;-,\beta}(t)d_{n'}^\beta(t)\Big]\,, \tag{8b}$$

with the interaction term

$$V_{n,n'}^{\gamma,\rho;\gamma',\rho'}(t) = \frac{q}{c}A\,w(t)\left(\delta_{n,n'-1} + \delta_{n,n'+1}\right) \cdot u_n^{\gamma,\rho\dagger}\left[\alpha_1\sin(\omega t) - \alpha_2\cos(\omega t)\right]u_n^{\gamma',\rho'}\,. \tag{9}$$

Note, that in the numerical simulation, the amplitude $|c_n^\alpha(t)|$ and $|d_n^\alpha(t)|$ is dropping exponentially for large $|n|$. Therefore we truncate the system of differential equations of the expansion coefficients and set them to zero for $|n| > 10$.

C. The numerical simulation and its spin properties

We demonstrate the possibility of filtering and polarizing the electron spin by a simulation of the eigensolutions's expansion coefficients $c_n^\sigma(t)$ and $d_n^\sigma(t)$, shown in Fig. 1. The electron spin is initially pointing upwards in the subfigures 1 (a) and 1 (b) and it initially points downwards in the Figures 1 (c) and 1 (d). One can see that spin-up electrons change their initial occupation probabilities $|c_{\pm1}(0)| = 1$ and $|c_{\mp1}(0)| = 0$ to the final probabilities $|c_{\pm1}(\tau)| = 0$ and $|c_{\mp1}(\tau)| = 1$, where

$$|c_n(t)|^2 = |c_n^\uparrow(t)|^2 + |c_n^\downarrow(t)|^2 \tag{10}$$

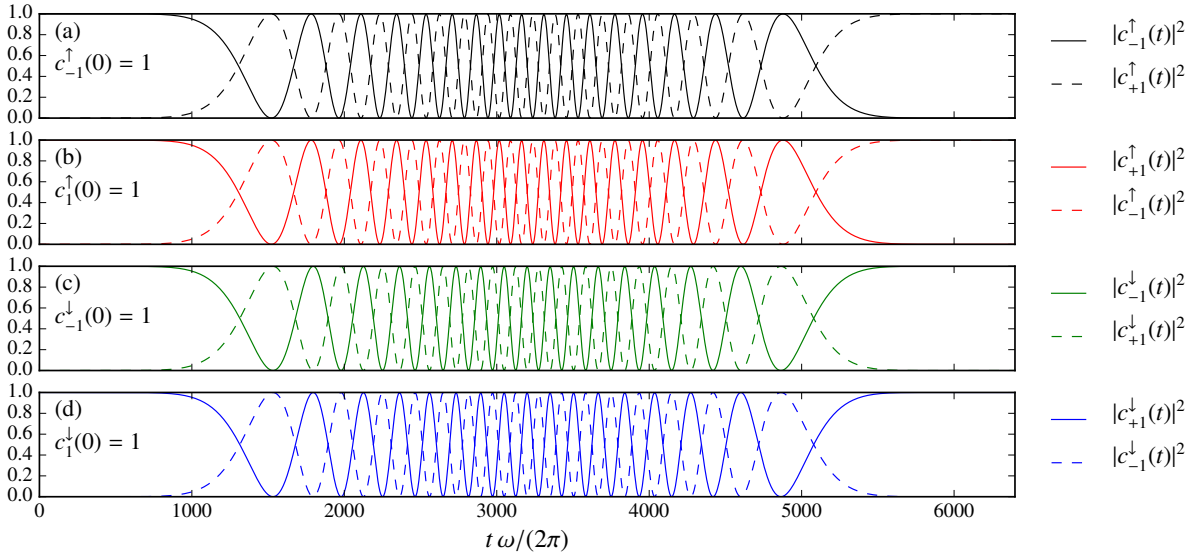

FIG. 1. (Color online) Simulated quantum dynamics. Shown are the absolute squares of the non-vanishing expansion coefficients of the wavefunction (7) over the time t. For the initial condition we set the the expansion coefficient $c^{\uparrow}_{-1}(0)$, $c^{\uparrow}_{1}(0)$, $c^{\downarrow}_{-1}(0)$ and $c^{\downarrow}_{1}(0)$ to one in the four subfigures (a), (b), (c) and (d) respectively, where all other expansion coefficients $c^{\sigma}_{n}(0)$ and $d^{\sigma}_{n}(0)$ are set to zero at time $t = 0$. One can see, that electrons with spin-up polarization are reversing their momentum, while the electrons with spin-down polarization are not changing their momentum. This means that spin-dependent diffraction is taking place. The laser peak intensity is $1.12 \times 10^{22}\,\mathrm{W/cm^2}$, with the wavelength $\lambda = 0.159\,\mathrm{nm}$ in our simulation, in accordance with the parameters used in [12].

is the probability of finding the electron with momentum $n\hbar k$ in z-direction at time t. In contrast, spin-down electrons are not exchanging their occupation probabilities between the momenta $\hbar k$ and $-\hbar k$. This spin-dependent diffraction behavior implies that it is possible to separate electrons according to their spin-state in the 2-photon Kapitza-Dirac effect with circularly polarized light.

Also, if the electron is initially moving upwards with momentum $\hbar k$, as in the subfigures 1 (b) and 1 (d) then the final electron will move downwards with electron spin pointing up or move upwards with electron spin pointing down. Similarly, an initially downwards moving electron as in the subfigures 1 (a) and 1 (c) will finally move upwards with spin pointing up or move downwards with spin pointing down. This means that the electron spin is polarized independent of its initial spin configuration.

The described spin dynamics are sketched in Fig. 2 for illustration.

III. APPROXIMATIVE DESCRIPTION

A simplified picture of the spin dynamics in the considered system can be given by an approximate analytic solution of the relativistic quantum dynamics, which is described by Erhard and Bauke [12]. The method makes use of a Foldy-Wouthuysen transformation of the Dirac equation for obtaining a non-relativistic approximation [18, 19]. The non-negligible contributions of the transformation can be written in terms of the Pauli equation plus a relativistic correction term

$$i\hbar\dot{\Psi}(\boldsymbol{x},t) = \left\{ \frac{1}{2m}\left[-i\hbar\boldsymbol{\nabla} - \frac{q}{c}\boldsymbol{A}(\boldsymbol{x},t)\right]^2 - \frac{q\hbar}{2mc}\boldsymbol{\sigma}\cdot\boldsymbol{B}(\boldsymbol{x},t) + \frac{q^2\hbar}{4m^2c^3}\boldsymbol{\sigma}\cdot[\boldsymbol{E}(\boldsymbol{x},t)\times\boldsymbol{A}(\boldsymbol{x},t)]\right\}\Psi(\boldsymbol{x},t)\,, \quad (11)$$

where a constant mc^2 contribution is neglected due to the possible elimination by choosing a suitable gauge. The electric and magnetic fields are related to the vector potential (2) by

$$\boldsymbol{E}(\boldsymbol{x},t) = -\frac{1}{c}\frac{\partial\boldsymbol{A}(\boldsymbol{x},t)}{\partial t} \quad \text{and} \quad (12)$$

$$\boldsymbol{B}(\boldsymbol{x},t) = \nabla\times\boldsymbol{A}(\boldsymbol{x},t)\,. \quad (13)$$

The approximation from Erhard and Bauke assumes a non-varying field amplitude $w(t) = 1$, for which the electric and magnetic fields evaluate to

$$\boldsymbol{E}(\boldsymbol{x},t) = 2A\,k\cos(kz)\,[\cos(\omega t)\boldsymbol{e}_x + \sin(\omega t)\boldsymbol{e}_y]\,, \quad (14a)$$

$$\boldsymbol{B}(\boldsymbol{x},t) = 2A\,k\sin(kz)\,[\cos(\omega t)\boldsymbol{e}_x + \sin(\omega t)\boldsymbol{e}_y]\,. \quad (14b)$$

In another step [12], Equation (11) can be solved with the Magnus expansion [20, 21], where terms which are negligible small and which are not growing linearly in time are neglected. The relevant terms of the calculation appear in an exponential representation of the time-

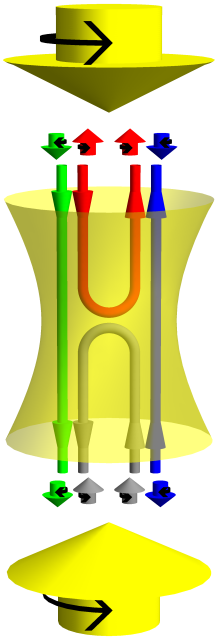

FIG. 2. (Color online) Interacting setup of laser and electron. Sketched in yellow arrows are two counter-propagating, co-rotating, circularly polarized laser beams from top and bottom and a corresponding yellow hyperboloid, which illustrates the resulting standing light wave. Depicted on the upper left and lower right are incoming spin-up and spin-down electrons, while on the lower left and the upper right are the outgoing electrons. The connecting lines of electrons indicate that momenta of spin-up electrons are reversed, while momenta of spin-down electrons remain unchanged by interaction with the laser field. This property is consistent with the simulation in Fig. 1. The diagram also coincides with the analytic expression (48) at time parameter $\eta = 8 \cdot 2\pi$, where η is defined in Eq. (37) (see also section IV E).

evolution and correspond to the wave equation

$$i\hbar\dot{\Psi}(\boldsymbol{x},t) = \left[\frac{1}{2m}\left(-i\hbar\boldsymbol{\nabla}\right)^2 + \frac{2q^2A^2}{mc^2}\cos^2(kz) - \frac{q^2A^2\hbar k}{m^2c^3}\left[\sin^2(kz) - \cos^2(kz)\right]\sigma_z\right]\Psi(\boldsymbol{x},t)\,. \quad (15)$$

One can exchange the relativistic wave function (7) of the Dirac equation by the two-component wave function

$$\Psi(\boldsymbol{x},t) = \sum_n c_n(t)e^{inkz}\,, \quad (16)$$

with the two-component structure

$$c_n(t) = \begin{pmatrix} c_n^{\uparrow}(t) \\ c_n^{\downarrow}(t) \end{pmatrix} \quad (17)$$

of expansion coefficients for the case of the Foldy-Wouthuysen transformed wave equation (11). Inserting the wave function (16) into the relativistic Pauli equation (15) and projecting on the plane-wave eigenfunctions $\chi^\sigma e^{inkz}$ yields

$$i\hbar\dot{c}_n(t) = \frac{n^2\hbar^2k^2}{2m}c_n(t) + \frac{q^2A^2}{2mc^2}\left[c_{n-2}(t) + 2c_n(t) + c_{n+2}(t)\right] + \frac{q^2A^2\hbar k}{2m^2c^3}\sigma_z\left[c_{n-2}(t) + c_{n+2}(t)\right]\,. \quad (18)$$

We restrict the system of differential equations to the electron momenta $-\hbar k$ and $\hbar k$, according to a similar description of the Kapitza-Dirac effect in the so-called Bragg regime, which is discussed by Batelaan [22–24], resulting in

$$i\dot{c}_{\pm1}(t) = (\Omega_k + 2\Omega_R)c_{\pm1}(t) + (\Omega_R\mathbf{1} + \Omega_S\sigma_z)c_{\mp1}(t)\,. \quad (19)$$

Analogous to [12], we have introduced the abbreviations for the kinetic energy

$$\Omega_k = \frac{\hbar k^2}{2m} \quad (20)$$

the Rabi frequency of the Kapitza-Dirac effect

$$\Omega_R = \frac{q^2A^2}{2mc^2\hbar}\,, \quad (21)$$

and the frequency of spin-dependent effects

$$\Omega_S = \Omega_R\frac{\hbar k}{mc}\,. \quad (22)$$

here. By choice of a suitable gauge, the term proportional to $(\Omega_k + 2\Omega_R)$ can be removed, yielding

$$i\dot{c}_{\pm1}(t) = (\Omega_R\mathbf{1} + \Omega_S\sigma_z)c_{\mp1}(t)\,. \quad (23)$$

By introducing the notion

$$c_{\pm1}(t) = T(t)c_{\pm1}(0) + R(t)c_{\mp1}(0) \quad (24)$$

for the time evolution one can write the solution of the differential equation Eq. (23) as

$$T(t) = \begin{pmatrix} \cos[(\Omega_R + \Omega_S)t] & 0 \\ 0 & \cos[(\Omega_R - \Omega_S)t] \end{pmatrix} \quad (25a)$$

$$R(t) = -i\begin{pmatrix} \sin[(\Omega_R + \Omega_S)t] & 0 \\ 0 & \sin[(\Omega_R - \Omega_S)t] \end{pmatrix}\,. \quad (25b)$$

Here, the matrices $R(t)$ and $T(t)$ describe spin-dependent initial- to final quantum state scattering with and without reversion of momentum, corresponding to reflection and transmission.

Note, that it is possible to solve the system of equations (23) also by accounting for the momenta $\pm3\hbar k$, instead of $\pm1\hbar k$ only [12], as explained in appendix B. One obtains corrections to the solution (25) which are negligibly small for the parameters in Fig. 1.

IV. PROPERTIES OF SPIN DYNAMICS

The matrices $T(t)$ and $R(t)$ in Eq. (25) can be represented in the form [9]

$$U_s(t) = \sqrt{P}e^{i\chi}\left[\cos\left(\frac{\xi}{2}\right)\mathbf{1} - i\sin\left(\frac{\xi}{2}\right)\boldsymbol{n}\cdot\boldsymbol{\sigma}\right]. \quad (26)$$

In case of real parameters P, χ, ξ and $\boldsymbol{n}$, where $\boldsymbol{n}$ is a unit vector, the term in the square bracket is an $\mathcal{SU}(2)$ rotation which rotates the electron spin. In this case P has the meaning of a spin-independent diffraction probability. In general the unit vector $\boldsymbol{n}$ can also be complex-valued, such that the representation (26) is parameterized by 8 independent parameters, corresponding to the 8 degrees of freedom of a complex valued 2×2 matrix [25]. In this more general case the term in the square bracket is no longer an $\mathcal{SU}(2)$ rotation and the parameter P looses it's property as spin-independent diffraction probability, because different spin-configurations will be diffracted with different probability.

We want to demonstrate this property for the time-propagation (25). The solution (25) consists of a fast dynamical part of scale Ω_R and a slow dynamical part of scale Ω_S which one can see from the expansion of the trigonometric functions

$$\begin{aligned}\cos\left[(\Omega_R \pm \Omega_S)t\right] &= \cos\Omega_R t\cos\Omega_S t \mp \sin\Omega_R t\sin\Omega_S t\\ \sin\left[(\Omega_R \pm \Omega_S)t\right] &= \sin\Omega_R t\cos\Omega_S t \pm \cos\Omega_R t\sin\Omega_S t\,.\end{aligned} \quad (27)$$

A. Instant Rabi-oscillations

We note that Ω_S is smaller than Ω_R by a factor of $\hbar k/(mc)$, ie. $\Omega_S \approx 0.015\,\Omega_R$ for the parameters used in the simulation of Fig. 1. Therefore, for times $t \ll 2\pi/\Omega_S$, the $\sin(\Omega_S t)$ term can be neglected and the $\cos(\Omega_S t)$ term can be set to one in Eq. (27), resulting in

$$T(t) \approx \begin{pmatrix}\cos\Omega_R t & 0\\ 0 & \cos\Omega_R t\end{pmatrix} \quad (28a)$$

and

$$R(t) \approx -i\begin{pmatrix}\sin\Omega_R t & 0\\ 0 & \sin\Omega_R t\end{pmatrix}. \quad (28b)$$

The matrix (26) can approximate $T(t)$ and $R(t)$ by setting

$$\xi = 0,\ P = \cos^2\Omega_R t \qquad \text{for } T(t) \text{ and} \quad (29a)$$

$$\xi = 0,\ P = \sin^2\Omega_R t \qquad \text{for } R(t)\,, \quad (29b)$$

corresponding to spin-independent Rabi-oscillations in the Kapitza-Dirac effect [24].

B. After an eighth of period $2\pi/\Omega_S$

The dynamics change, when the product $\Omega_S t$ reaches fractions of the period 2π. An interesting value is an eighth of the period $2\pi/\Omega_S$, which also corresponds to the final quantum state configuration of the simulation in Fig. 1, as explained in section IV E. Therefore we introduce the shifted time

$$t' = t - \frac{\pi}{4\Omega_S}\,. \quad (30)$$

The functions $\cos\Omega_S t$ and $\sin\Omega_S t$ evaluate to $1/\sqrt{2}$ for $|t'| \ll \Omega_S/(2\pi)$ in the trigonometric expansion (27), resulting in the non-vanishing matrix elements

$$\begin{aligned}T_{11}(t) &\approx [\cos(\Omega_R t' + \varphi_0) - \sin(\Omega_R t' + \varphi_0)]/\sqrt{2}\\ T_{22}(t) &\approx [\cos(\Omega_R t' + \varphi_0) + \sin(\Omega_R t' + \varphi_0)]/\sqrt{2}\\ R_{11}(t) &\approx -i[\sin(\Omega_R t' + \varphi_0) + \cos(\Omega_R t' + \varphi_0)]/\sqrt{2}\\ R_{22}(t) &\approx -i[\sin(\Omega_R t' + \varphi_0) - \cos(\Omega_R t' + \varphi_0)]/\sqrt{2}\end{aligned} \quad (31)$$

where we introduce the abbreviation

$$\varphi_0 = \frac{\pi}{4}\frac{\Omega_R}{\Omega_S}\,. \quad (32)$$

The matrices (31) can be expressed in terms of the spin approximation $U_s(t)$ in Eq. (26), by using the parameters

$$P = 1/2\,,\quad \chi = 0\,,\quad \boldsymbol{n} = (0,0,-i)^T\,, \quad (33a)$$

$$\xi = 2\Omega_R t' + 2\varphi_0 \quad \text{for } T(t) \quad (33b)$$

and

$$P = 1/2\,,\quad \chi = 3\pi/2\,,\quad \boldsymbol{n} = (0,0,-i)^T\,, \quad (33c)$$

$$\xi = 2\Omega_R t' + 2\varphi_0 - \pi \quad \text{for } R(t)\,. \quad (33d)$$

The matrix in the square brackets in Eq. (26) is no longer an $\mathcal{SU}(2)$ matrix, for the set of parameters in Eq. (33), because the vector $\boldsymbol{n}$ is imaginary-valued now. It implies that the diffraction probability depends on the electron's spin-configuration, where spin-dependent diffraction is characterized as a non-unitary propagation matrix of the electron spin.

For investigating the spin properties of the diffraction process, it is suitable to shift the time (30) further by the small value $\pi/(4\Omega_R)$. Therefore, we introduce the shifted time

$$t'' = t - \frac{\pi}{4\Omega_R} - \frac{\pi}{4\Omega_S}\,. \quad (34)$$

Inserting this shifted time in the arguments of the trigonometric functions (25) yields

$$\Omega_R t + \Omega_S t = \Omega_R t'' + \varphi_0 + \Omega_S\left(t'' + \frac{\pi}{4\Omega_R}\right) + \frac{\pi}{2} \quad (35a)$$

$$\Omega_R t - \Omega_S t = \Omega_R t'' + \varphi_0 - \Omega_S\left(t'' + \frac{\pi}{4\Omega_R}\right). \quad (35b)$$

The term $\Omega_S[t'' + \pi/(4\Omega_R)]$ is negligibly small for times $|t''| \ll 2\pi/\Omega_S$ and can be omitted, such that the matrices $T(t)$ and $R(t)$ in (25) can be written as

$$T(t) \approx \begin{pmatrix} -\sin\eta & 0 \\ 0 & \cos\eta \end{pmatrix}, \quad R(t) \approx -i \begin{pmatrix} \cos\eta & 0 \\ 0 & \sin\eta \end{pmatrix}, \tag{36}$$

where the argument of the trigonometric functions is abbreviated with

$$\eta = \Omega_R t'' + \varphi_0 \,. \tag{37}$$

The parameterization of $U_s(t)$ for Eq. (36) is analogous to Eq. (33), where only ξ needs to be exchanged and be expressed in terms of t'', yielding

$$\xi = 2\Omega_R t'' + 2\varphi_0 + \pi/2 \,, \tag{38a}$$

instead of Eq. (33b) for $R(t)$ and

$$\xi = 2\Omega_R t'' + 2\varphi_0 - \pi/2 \tag{38b}$$

instead of Eq. (33d) for $T(t)$.

C. Spin-dependent diffraction

We want to illustrate the spin properties of the spin propagation matrices $T(t)$ and $R(t)$ in Eq. (36) and assume the quantum state

$$c_{-1}(0) = \begin{pmatrix} \cos\frac{\theta}{2} \\ \sin\frac{\theta}{2} e^{i\varphi} \end{pmatrix}, \qquad c_1(0) = 0 \tag{39}$$

for the initial configuration of the electron. This corresponds to an electron which moves with momentum $-\hbar k$ in z-direction. The Bloch state parameterization of $c_{-1}(0)$ corresponds to the Bloch vector as sketched in Fig. 3. Inserting the initial state and the matrices (36) into the time-evolution (24) results in the final quantum states

$$c_1(t) = \begin{pmatrix} -i\cos\eta\cos\frac{\theta}{2} \\ -i\sin\eta\sin\frac{\theta}{2} e^{i\varphi} \end{pmatrix} \tag{40a}$$

for the diffracted electron wavefunction and

$$c_{-1}(t) = \begin{pmatrix} -\sin\eta\cos\frac{\theta}{2} \\ \cos\eta\sin\frac{\theta}{2} e^{i\varphi} \end{pmatrix} \tag{40b}$$

for the undiffracted electron wavefunction. Consequently, one can compute the probabilities

$$|c_{\pm 1}(t)|^2 = \frac{1}{2}\left(1 \pm \cos\theta\cos 2\eta\right) , \tag{41}$$

of finding the electron moving in positive or negative z-direction. Eq. (41) implies a time-dependence of the diffraction probability by the time-parameter η and also a dependence on the original azimutal spin-orientation θ. We are plotting the diffraction probability $|c_1(t)|^2$ in Fig. 4(a). The chosen period of time from $2250\,\omega/(2\pi)$ till $2550\,\omega/(2\pi)$ corresponds to the one Rabi period $2\pi/\Omega_R$, starting and ending approximately at the parameter values $\eta \approx 7.5$ and $\eta \approx 8.5$, respectively. In Fig. 4(b) we also plot the diffraction probability of the time-propagation (B16) of the quantum state (39) for comparison. Eq. (B16) is the most accurate available analytic approximation [12]. Furthermore, we plot the numerically simulated time-evolution of the quantum state (39) by using the relativistic equations of motion (8) and the commonly used envelope function [8–12, 16, 17]

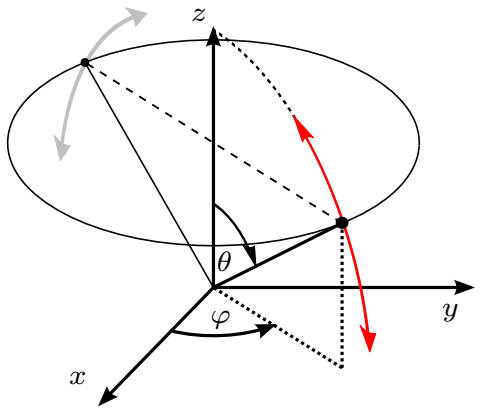

FIG. 3. (Color online) Bloch vector in our setup. Shown is the expectation value of the quantum state (39) with respect to the vector $\boldsymbol{\sigma}$ of Pauli matrices, being the Bloch vector, which points in the direction (θ, φ) in spherical coordinates. The change of the vector's z-component due to the laser-electron interaction in Fig. 5 is indicated by the dark gray (red) arrows in this sketch. The dashed line shows an additional reversion of the Bloch vector's x-y component, implied by Eq. (44).

$$w(t) = \begin{cases} \sin^2\frac{\pi t}{2\,\delta\tau} & \text{if } 0 \le t \le \delta\tau \\ 1 & \text{if } \delta\tau \le t \le \tau - \delta\tau \\ \sin^2\frac{\pi(\tau - t)}{2\,\delta\tau} & \text{if } \tau - \delta\tau \le \tau \,, \end{cases} \tag{42}$$

in Fig. 4(c). Different simulations with different parameters τ are carried out for each time t in Fig. 4(c) and the simulation results $|c_n(\tau)|^2$ at the end of every simulation are plotted. For all simulations we set $\delta\tau = 10\pi/\omega$.

The nice agreement of Fig. 4(a) with Fig. 4(b) and Fig. 4(c) indicates, that the analytic solution (25) describes the spin-dynamics well in the chosen period of time. One can see a small retardation of the numeric solution in Fig. 4(c), as compared to the analytic solutions in Fig. 4(a) and Fig. 4(b) of 7.7 laser cycles. This retardation can be explained by the switch on and switch of process of the external field, as discussed in appendix A. In fact, if one inserts $\delta\tau = 10\pi/\omega$ in Eq. (A7) one obtains a retardation of the scaled time by 6.3 laser cycles.

The quantum dynamics shown here differs fundamentally from previous investigations [8–11, 13] of the Kapitza-Dirac effect in which the propagation of the elec-

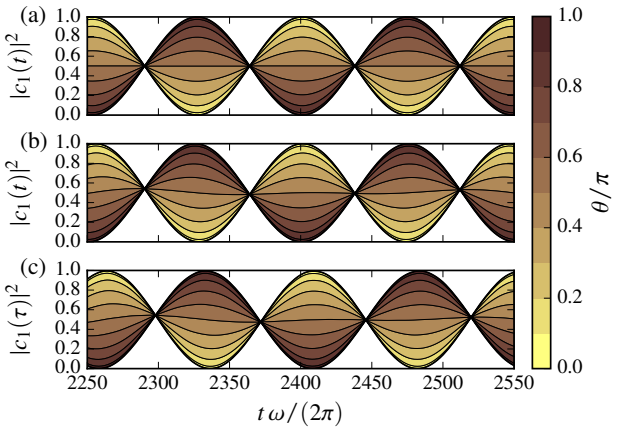

FIG. 4. (Color online) Spin-dependent diffraction probability. The diffraction probability (10) of finding an electron with initial state (39) at final momentum $\hbar k$ is plotted over time. The initial quantum state is evolved in time by the approximation (36) in subplot (a), by the more accurate approximation (B16) in subplot (b) and by a numerical solution according to the differential equations (8) in subplot (c). One can see that the diffraction probability depends on the initial spin configuration of the electron, where $\theta = 0$ corresponds to spin-up and $\theta = \pi$ corresponds to spin-down.

tron spin could be described by the matrix $U_s(t)$ in Eq. (26) with a real-valued unit vector $\boldsymbol{n}$. For example, if the vector $\boldsymbol{n}$ in the set of the approximation parameters (33c) and (38b) had the value $(0, 0, -1)^T$, the final quantum state of the diffracted electron would be

$$c_1(t) = -\frac{i}{\sqrt{2}} \begin{pmatrix} \cos\frac{\theta}{2} e^{i\frac{\xi}{2}} \\ \sin\frac{\theta}{2} e^{i\varphi - i\frac{\xi}{2}} \end{pmatrix} \tag{43}$$

instead of (40a). Then, the diffraction probability would have the time-independent and also spin in-dependent value $|c_1(t)|^2 = 1/2$. In contrast to that, the diffraction probability is time- and spin-dependent in Fig. 4. This property can be used to separate spin-up from spin-down electrons in form of a spin filter.

D. Polarization of the electron spin

The expectation value of the final quantum state (40a) with respect to the Pauli spin matrices is

$$c_1(t)^\dagger \sigma_x c_1(t) = \frac{1}{2} \sin\theta \sin 2\eta \cos\varphi \tag{44a}$$

$$c_1(t)^\dagger \sigma_y c_1(t) = \frac{1}{2} \sin\theta \sin 2\eta \sin\varphi \tag{44b}$$

$$c_1(t)^\dagger \sigma_z c_1(t) = \frac{1}{2} \left(\cos\theta + \cos 2\eta\right) . \tag{44c}$$

This can be normalized by the diffraction probability $|c_1(t)|^2$ of Eq. (41) and results in the Bloch vector

$$\langle \boldsymbol{n}(t) \rangle = \frac{c_1(t)^\dagger \boldsymbol{\sigma} c_1(t)}{|c_1(t)|^2} \tag{45}$$

of the electron spin of the diffracted electron. The z-component of the Bloch vector (45) is plotted in Fig. 5(a). We also plot the z-component of the Bloch vector resulting from the time-propagation (B16) of the initial quantum state (39) in Fig. 5(b), which is similar to Fig. 4(b). Also the z-component of the Bloch vector from the numerical propagation of the relativistic equations of motion (8) is plotted in Fig. 5(c), according to the same procedure as for Fig. 4(c).

The subplots in Fig. 5 agree similarly as described for the subplots in Fig. 4. This again emphasizes that Eq. (25) is a suitable solution of the quantum dynamics in the chosen time period and also confirms the identified retardation (A7) due to the switch on and switch off process of the external field.

In analogy to the diffraction probability, the shown dynamics of the spin-direction of the electron is fundamentally different from dynamics which is related to a real-valued unit vector $\boldsymbol{n}$ in Eq. (26). For example the Bloch vector

$$c_1(t)^\dagger \sigma_x c_1(t) = -\frac{1}{2} \sin\theta \sin(\varphi - 2\eta) \tag{46a}$$

$$c_1(t)^\dagger \sigma_y c_1(t) = \frac{1}{2} \sin\theta \cos(\varphi - 2\eta) \tag{46b}$$

$$c_1(t)^\dagger \sigma_z c_1(t) = \frac{1}{2} \cos\theta\,, \tag{46c}$$

of the assumed quantum state (43) is rotating with angular velocity $-2\Omega_R$ around the z-axis. In contrast to that, the z-component of the electron's spin vector is periodically tilted upwards and downwards in Fig. 5, as sketched by the red arrows in Fig. 3. At certain times, for example at $t \approx 2400 \cdot 2\pi/\omega$ or $t \approx 2450 \cdot 2\pi/\omega$ the electron is always pointing upwards or downwards respectively, independent of its initial polarization in the z-direction. Therefore, it is possible to polarize an initially unpolarized electron spin.

Still, the vector of spin expectation values (44) is flipping it's direction in the x-y-plane with period π/Ω_R. This flipping is sketched for illustration as dashed line in Fig. 3. Hence, the spin-flipping dynamics in the x-y-plane goes along with spin-polarizing and spin-filtering effects along the z-direction, in accordance with dynamics reported by Erhard and Bauke [12], if one accounts for the choice of laser geometry.

E. Distinct spin separation

For $\eta = \pi n,\ n \in \mathbb{N}$ the approximate solution (36) implies that spin-up electrons will be diffracted with momentum reversal in z-direction with probability 1 and, likewise, spin-down electrons will remain in their motional state with probability 1. The reversed property, ie. diffraction of spin-down electrons with probability 1 and no diffraction of spin-up electrons with probability 1, is reached for $\eta = \pi/2 + \pi n,\ n \in \mathbb{N}$.

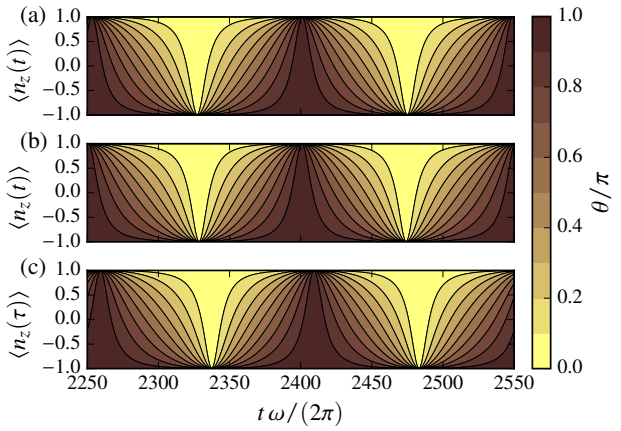

FIG. 5. (Color online) Polarization of the electron spin. The z-component of the Bloch vector (45) is plotted over time. Similarly as for Fig. 4, the initial quantum state (39) is evolved in time by the approximation (36) in subplot (a), by the more accurate approximation (B16) in subplot (b) and by a numerical solution according to the differential equations (8) in subplot (c). One can observe, that $\langle \boldsymbol{n}(t)\rangle$ is pointing upwards and downwards periodically, implying that the electron spin can be polarized.

Fig. 4 and Fig. 5 suggest that Eq. (36) is a good approximation for the value $\eta = 8 \cdot 2\pi$. This is indeed the case, because one can compute

$$t'' = \frac{16\pi - \varphi_0}{\Omega_R} \approx -0.18 \cdot \frac{2\pi}{\Omega_R}\,, \tag{47}$$

for $\eta = 8 \cdot 2\pi$. Then, the necessary condition $|t''| \ll 2\pi/\Omega_S$, which is the requirement that Eq. (36) is a good approximation, is fulfilled well. In the case of $\eta = 8 \cdot 2\pi$ one obtains

$$T(t) = \begin{pmatrix} 0 & 0 \\ 0 & 1 \end{pmatrix}\,, \qquad R(t) = \begin{pmatrix} -i & 0 \\ 0 & 0 \end{pmatrix}\,, \tag{48}$$

for the matrices (36). The action of $T(t)$ and $R(t)$ at the initial conditions in Fig. 1 is resulting in the corresponding final configurations in all four subfigures of Fig. 1, as illustrated in Fig. 2. In other words Eq. (48) displays the propagation matrix of the quantum dynamics in Fig. 1 and its illustration in Fig. 2.

Note, that the time t in Eq. (48) is related to η by Eq. (34) and Eq. (37) and evaluates to

$$t = \frac{\eta}{\Omega_R} + \frac{\pi}{4\Omega_R} = 2401.1\frac{\omega}{2\pi} = 1.27\,\mathrm{fs}\,. \tag{49}$$

This differs from the total interaction time τ of the dynamics in Fig. 1 which is 6399 laser cycles. The reason is the usage of a plateau shaped envelope function (42) for the simulation in Fig. 4(c) and Fig. 5(c) as compared to the Gaussian shaped envelope function (3) in Fig. 1. It is possible to associate the different field envelopes by a substitution technique which is discussed in appendix A. We obtain $\tilde{t}(\tau) = 2399.6\,\omega/(2\pi)$ from Eq. (A6) which is fitting to the time in Eq. (49). This demonstrates that the considerations in appendix A are suitable for relating the quantum dynamics of different time-dependent field amplitudes to each other.

The matrices $T(t)$ and $R(t)$ in Eq. (48) can be expressed in terms of $U_s(t)$ in Eq. (26) by the parameters (33a) with $\xi = \pi/2$ and (33c) with $\xi = -\pi/2$, respectively. For any set of parameters, the matrices in Eq. (48) could only be approximated by $U_s(t)$ if an imaginary valued unit vector $\boldsymbol{n}$ was used. In contrast to that, the spin-dynamics as described in the references [8–11, 13] would require a real-valued unit vector $\boldsymbol{n}$ for the parameterization in terms of $U_s(t)$. The real-valued unit vector $\boldsymbol{n}$ implies that the absolute values of all eigenvalues of $U_s(t)$ have the same value $\sqrt{P}$. For the imaginary unit vector $\boldsymbol{n}$ in the representation of $U_s(t)$ the absolute values of the eigenvalues are 0 and 1, as for the matrices $T(t)$ and $R(t)$ in Eq. (48). In other words $T(t)$ and $R(t)$ are projection matrices times a complex phase. This property differs fundamentally from the unitary propagation of the electron spin in previous descriptions of spin-dynamics in the Kapitza-Dirac effect.

We point out that it is possible to identify similar properties for the quantum state propagation of an electron in a phase-grating [14]. Also, spin-dependent electron scattering in a recently proposed, bi-chromatic, interferometric beam splitter [15] can be described in terms of a non-unitary spin propagation.

V. CONCLUSION

The effect, which is described in this article allows for the polarization and spin-detection of free electrons due to interaction with a standing, circularly polarized light wave only. The quantum treatment of our theory prediction challenges Pauli's conjecture on the unfeasibility of electron spin separation which was based on an argument of classical trajectories. Our results are presented in the context of high intensity X-ray laser beams of novel facilities, for which the feasibility of electron diffraction with spin effects at similar parameters has been discussed already in an earlier investigation [8]. More details on the experimental feasibility are also considered in [15]. Furthermore, the experimental community discusses the implementation of spin-dependent electron scattering with light in the optical regime [26] and a perturbative variant is possible in terms of higher order Compton scattering in the high energy regime [27–29]. Since the effect is also sensitive on the pulse amplitude and pulse duration of the laser field it could be useful for beam diagnosis. Finally, we point out that the propagation of the quantum state is described by a unitary transformation. Therefore, the effect can be reversed, provided that a high fidelity experimental setup is available. We conclude a non-destructive spin-filter, which might be even suitable for ultrafast quantum computation with the spin of entangled free electrons [30].

Acknowledgements

S.A. thanks for help and feedback from Shi-Yao Zhu, Chang-Pu Sun, Tilen Cadez, Heiko Bauke and Carsten Müller. This work has been supported by the NSFC Grant No. 11650110442.

Appendix A: The effect of the time-dependent field amplitude

Assume the constant field amplitude A would be replaced by the time-dependent amplitude $A\,w(t)$ in Eq. (23), with corresponding time-dependent frequencies

$$\Omega_R(t) = \Omega_R\, w(t)^2 \quad \text{and} \quad \Omega_S(t) = \Omega_S\, w(t)^2\,. \tag{A1}$$

Then $w(t)$ is just appearing as time-dependent prefactor of the coefficients of the differential equation

$$i\dot{c}_{\pm1}(t) = w(t)^2(\Omega_R\mathbf{1} + \Omega_S\sigma_z)c_{\mp1}(t)\,. \tag{A2}$$

We want to transform this equation to a formally equivalent version of Eq. (23) with reparameterized coefficients $\tilde{c}\left(\tilde{t}\right)$ of a scaled time

$$\tilde{t}(t) = \int_0^t w(s)^2 ds\,, \tag{A3}$$

such that $c(t) = \tilde{c}\left(\tilde{t}(t)\right)$. Such a scaled time corresponds to the warped time parameter [25] or the the action parameter [16]. The new coefficients imply

$$\begin{aligned}\dot{c}_n(t) = \frac{\partial}{\partial t}c_n(t) &= \frac{\partial}{\partial t}\tilde{c}_n\left(\tilde{t}(t)\right) \\ &= \frac{\partial\tilde{t}(t)}{\partial t}\frac{\partial}{\partial\tilde{t}}\tilde{c}_n\left(\tilde{t}\right) = w(t)^2\frac{\partial}{\partial\tilde{t}}\tilde{c}_n\left(\tilde{t}\right)\end{aligned} \tag{A4}$$

due to the inner derivative. Plugging this back into (A2) results in

$$i\frac{\partial}{\partial\tilde{t}}\tilde{c}\left(\tilde{t}\right) = (\Omega_R\mathbf{1} + \Omega_S\sigma_z)\tilde{c}_{\mp1}\left(\tilde{t}\right) \tag{A5}$$

which is formally equivalent to Eq. (23), as desired. Integrating the scaled time for the whole interaction time τ yields the time

$$\tilde{t}(\tau) = \int_0^\tau w(s)^2 ds = \int_0^\tau \sin^4\left(\frac{\pi s}{\tau}\right) ds = \frac{3}{8}\tau\,, \tag{A6}$$

for the Gaussian envelope function (3). For the plateau-shaped envelope function (42) one obtains

$$\tilde{t}(\tau) = \int_0^\tau w(s)^2 ds = \tau - \frac{5}{4}\delta\tau \tag{A7}$$

in a similar calculation.

Appendix B: Comparison with more accurate solution

We want to compare the approximative solution (25) of section III with the solution given in [12] which also accounts for the electron momenta $3\hbar$ and $-3\hbar k$. By performing an analog derivation, the differential equation (18) can first be written in matrix notion as

$$i\begin{pmatrix}\dot{c}_{-3}\\ \dot{c}_{-1}\\ \dot{c}_1\\ \dot{c}_3\end{pmatrix} = \begin{pmatrix}9\Omega_k\mathbf{1} & M & 0 & 0\\ M & \Omega_k\mathbf{1} & M & 0\\ 0 & M & \Omega_k\mathbf{1} & M\\ 0 & 0 & M & 9\Omega_k\mathbf{1}\end{pmatrix}\begin{pmatrix}c_{-3}\\ c_{-1}\\ c_1\\ c_3\end{pmatrix} \tag{B1}$$

with the spin-dependent coupling matrix

$$M = \Omega_R\mathbf{1} + \Omega_S\sigma_z = \begin{pmatrix}\Omega_R+\Omega_S & 0\\ 0 & \Omega_R-\Omega_S\end{pmatrix}. \tag{B2}$$

A constant from the ponderomotive potential, which causes a global phase with oscillation frequency $2\Omega_R$ can be omitted by choice of a suitable gauge. Similarly as in reference [12], we use a computer algebra system and a simplification for expressions of the form

$$\begin{aligned}&\sqrt{\left[8\Omega_k - (\Omega_R+\Omega_S)\right]^2 + 4(\Omega_R+\Omega_S)^2}\\ &\qquad = 8\Omega_k - \Omega_R - \Omega_S + \frac{(\Omega_R+\Omega_S)^2}{4\Omega_k} + \dots\,,\end{aligned} \tag{B3}$$

for the case of small frequencies $\Omega_R \ll \Omega_k$ and $\Omega_S \ll \Omega_k$ and therewith small numbers Ω_R/Ω_k and Ω_S/Ω_k. For the matrix in Eq. (B1), we obtain the approximated eigenenergies

$$\epsilon_1 \approx \epsilon_0 + \Omega_R + \Omega_S - \Delta \tag{B4a}$$
$$\epsilon_2 \approx \epsilon_0 - \Omega_R + \Omega_S + \Delta \tag{B4b}$$
$$\epsilon_3 \approx \epsilon_0 + \Omega_R - \Omega_S + \Delta \tag{B4c}$$
$$\epsilon_4 \approx \epsilon_0 - \Omega_R - \Omega_S - \Delta \tag{B4d}$$
$$\epsilon_5 \approx \epsilon_0 + 8\Omega_k - \Delta \tag{B4e}$$
$$\epsilon_6 \approx \epsilon_0 + 8\Omega_k + \Delta \tag{B4f}$$
$$\epsilon_7 \approx \epsilon_0 + 8\Omega_k + \Delta \tag{B4g}$$
$$\epsilon_8 \approx \epsilon_0 + 8\Omega_k - \Delta\,, \tag{B4h}$$

where we have introduced the frequency of an energy shift

$$\epsilon_0 = \Omega_k - \frac{\Omega_R^2 + \Omega_S^2}{8\Omega_k} \tag{B5}$$

and the frequency of higher order corrections of the quantum dynamics

$$\Delta = \frac{\Omega_R\Omega_S}{4\Omega_k}\,. \tag{B6}$$

The frequency ϵ_0 will be omitted in the following calculation, as it causes an additional, time-dependent phase of the quantum system (B1) which can be removed by choice of a suitable gauge. The corresponding approximated eigenvectors of the eigenvalues (B4) are

$$\boldsymbol{v}_1 = \left(1, 0, -\frac{8\Omega_k}{\Omega_R+\Omega_S}+1-\frac{\Omega_R+\Omega_S}{8\Omega_k}, 0, -\frac{8\Omega_k}{\Omega_R+\Omega_S}+1-\frac{\Omega_R+\Omega_S}{8\Omega_k}, 0, 1, 0\right)^T \tag{B7a}$$

$$\boldsymbol{v}_2 = \left(0, -1, 0, \frac{8\Omega_k}{\Omega_R-\Omega_S}+1-\frac{-\Omega_R+\Omega_S}{8\Omega_k}, 0, -\frac{8\Omega_k}{\Omega_R-\Omega_S}-1+\frac{-\Omega_R+\Omega_S}{8\Omega_k}, 0, 1\right)^T \tag{B7b}$$

$$\boldsymbol{v}_3 = \left(0, 1, 0, -\frac{8\Omega_k}{\Omega_R-\Omega_S}+1+\frac{-\Omega_R+\Omega_S}{8\Omega_k}, 0, -\frac{8\Omega_k}{\Omega_R-\Omega_S}+1+\frac{-\Omega_R+\Omega_S}{8\Omega_k}, 0, 1\right)^T \tag{B7c}$$

$$\boldsymbol{v}_4 = \left(-1, 0, \frac{8\Omega_k}{\Omega_R+\Omega_S}+1+\frac{\Omega_R+\Omega_S}{8\Omega_k}, 0, -\frac{8\Omega_k}{\Omega_R+\Omega_S}-1-\frac{\Omega_R+\Omega_S}{8\Omega_k}, 0, 1, 0\right)^T \tag{B7d}$$

$$\boldsymbol{v}_5 = \left(1, 0, \frac{\Omega_R+\Omega_S}{8\Omega_k}, 0, \frac{\Omega_R+\Omega_S}{8\Omega_k}, 0, 1, 0\right)^T \tag{B7e}$$

$$\boldsymbol{v}_6 = \left(0, -1, 0, \frac{-\Omega_R+\Omega_S}{8\Omega_k}, 0, -\frac{-\Omega_R+\Omega_S}{8\Omega_k}, 0, 1\right)^T \tag{B7f}$$

$$\boldsymbol{v}_7 = \left(0, 1, 0, \frac{\Omega_R-\Omega_S}{8\Omega_k}, 0, \frac{\Omega_R-\Omega_S}{8\Omega_k}, 0, 1\right)^T \tag{B7g}$$

$$\boldsymbol{v}_8 = \left(-1, 0, \frac{\Omega_R+\Omega_S}{8\Omega_k}, 0, -\frac{\Omega_R+\Omega_S}{8\Omega_k}, 0, 1, 0\right)^T . \tag{B7h}$$

For the limit $\Omega_k \gg \Omega_R > \Omega_S$ as used in [12], the eigenvectors are approximated by

$$(\boldsymbol{v}_1, \boldsymbol{v}_2, \boldsymbol{v}_3, \boldsymbol{v}_4, \boldsymbol{v}_5, \boldsymbol{v}_6, \boldsymbol{v}_7, \boldsymbol{v}_8) = \frac{1}{\sqrt{2}} \begin{pmatrix} 0 & 0 & 0 & 0 & 1 & 0 & 0 & 1 \\ 0 & 0 & 0 & 0 & 0 & 1 & 1 & 0 \\ 1 & 0 & 0 & 1 & 0 & 0 & 0 & 0 \\ 0 & 1 & 1 & 0 & 0 & 0 & 0 & 0 \\ 1 & 0 & 0 & -1 & 0 & 0 & 0 & 0 \\ 0 & -1 & 1 & 0 & 0 & 0 & 0 & 0 \\ 0 & 0 & 0 & 0 & 1 & 0 & 0 & -1 \\ 0 & 0 & 0 & 0 & 0 & -1 & 1 & 0 \end{pmatrix}, \tag{B8}$$

and normalized to 1 here. We are interested in the time-evolution of the quantum states $c_1(t)$ and $c_{-1}(t)$ and point out that the first 4 approximated eigenvectors in Eq. (B8) form a closed subspace of these states. Within this subspace, the time-evolution of the vector of expansion coefficients

$$C(t) = \left(c_{-1}^{\uparrow}(t), c_{-1}^{\downarrow}(t), c_1^{\uparrow}(t), c_1^{\downarrow}(t)\right)^T \tag{B9}$$

has an equivalent expression for the time-evolution (24) and can be written as $C(t) = U(t)C(0)$ with the form of the propagator

$$U(t) = \begin{pmatrix} T(t) & R(t) \\ R(t) & T(t) \end{pmatrix} . \tag{B10}$$

The time-evolution can be computed by making use of the matrix exponential

$$U(t) = V e^{-iDt} V^{-1} , \tag{B11}$$

in which we are using the eigenvector subspace matrix

$$V = V^{-1\dagger} = \frac{1}{\sqrt{2}} \begin{pmatrix} 1 & 0 & 0 & 1 \\ 0 & 1 & 1 & 0 \\ 1 & 0 & 0 & -1 \\ 0 & -1 & 1 & 0 \end{pmatrix} \tag{B12}$$

and the corresponding diagonal matrix of eigenvalues $D = \mathrm{diag}(\epsilon_1, \epsilon_2, \epsilon_3, \epsilon_4)$. From the property $U(t)^\dagger U(t) = \mathrm{id}_4$ we note that

$$|T|^2 + |R|^2 = \mathbf{1} \tag{B13}$$

$$T^\dagger R + R^\dagger T = 0 \tag{B14}$$

holds, where id_4 is the 4×4 identity matrix. Thus $R(t)$ and $T(t)$ are reflection and transmission matrices.

An explicit expression of $U(t)$ is

$$U(t) = \frac{1}{2}\begin{pmatrix} e^{-i\epsilon_1 t} + e^{-i\epsilon_4 t} & 0 & e^{-i\epsilon_1 t} - e^{-i\epsilon_4 t} & 0 \\ 0 & e^{-i\epsilon_2 t} + e^{-i\epsilon_3 t} & 0 & -e^{-i\epsilon_2 t} + e^{-i\epsilon_3 t} \\ e^{-i\epsilon_1 t} - e^{-i\epsilon_4 t} & 0 & e^{-i\epsilon_1 t} + e^{-i\epsilon_4 t} & 0 \\ 0 & -e^{-i\epsilon_2 t} + e^{-i\epsilon_3 t} & 0 & e^{-i\epsilon_2 t} + e^{-i\epsilon_3 t} \end{pmatrix}, \tag{B15}$$

from which one can read off the matrices

$$T(t) = \mathrm{diag}(\cos[(\Omega_R + \Omega_S)t]e^{-i\Delta t}, \cos[(\Omega_R - \Omega_S)t]e^{i\Delta t}), \tag{B16a}$$

$$R(t) = \mathrm{diag}(-i\sin[(\Omega_R + \Omega_S)t]e^{-i\Delta t}, -i\sin[(\Omega_R - \Omega_S)t]e^{i\Delta t}). \tag{B16b}$$

Note again, that ϵ_0 has been omitted here.

The frequency Δ scales with the fourth power of the field amplitude A, while Ω_R and Ω_S only scale with the square of A. Therefore, for small fields the frequency Δ is smaller than Ω_R and Ω_S, which is the case for the parameters chosen in Fig. 1. Thus, one may approximate

$$e^{i\Delta t} \approx 1 + i\Delta t \approx 1 \tag{B17}$$

on time scales which are much shorter than the period $2\pi/\Delta$. In this case, the matrices $T(t)$ and $R(t)$ in (B16) change into the simpler solution (25) of section III.

[1] M. Morrison, Stud. Hist. Phil. Sci. B **38**, 529 (2007).
[2] W. Gerlach and O. Stern, Z. Phys. **8**, 110 (1922).
[3] W. Pauli, Proc. Sixth Solvay Conf. , 183,217,275 (1932).
[4] H. Dehmelt, Proc. Nat. Acad. Sci. U.S.A. **83**, 2291 (1986).
[5] D. L. Freimund and H. Batelaan, Laser Phys. **13**, 892 (2003).
[6] D. L. Freimund, K. Aflatooni, and H. Batelaan, Nature (London) **413**, 142 (2001).
[7] P. L. Kapitza and P. A. M. Dirac, Math. Proc. Cambridge Philos. Soc. **29**, 297 (1933).
[8] S. Ahrens, H. Bauke, C. H. Keitel, and C. Müller, Phys. Rev. Lett. **109**, 043601 (2012).
[9] S. Ahrens, H. Bauke, C. H. Keitel, and C. Müller, Phys. Rev. A **88**, 012115 (2013).
[10] H. Bauke, S. Ahrens, C. H. Keitel, and R. Grobe, New J. Phys. **16**, 103028 (2014).
[11] H. Bauke, S. Ahrens, and R. Grobe, Phys. Rev. A **90**, 052101 (2014).
[12] R. Erhard and H. Bauke, Phys. Rev. A **92**, 042123 (2015).
[13] M. M. Dellweg, H. M. Awwad, and C. Müller, Phys. Rev. A **94**, 022122 (2016).
[14] S. McGregor, R. Bach, and H. Batelaan, New J. Phys. **13**, 065018 (2011).
[15] M. M. Dellweg and C. Müller, arXiv:1607.08793.
[16] M. M. Dellweg and C. Müller, Phys. Rev. A **91**, 062102 (2015).
[17] M. M. Dellweg and C. Müller, J. Phys.: Conf. Ser. **594**, 012015 (2015).
[18] L. L. Foldy and S. A. Wouthuysen, Phys. Rev. **78**, 29 (1950).
[19] J. Fröhlich and U. M. Studer, Rev. Mod. Phys. **65**, 733 (1993).
[20] W. Magnus, Commun. Pure Appl. Math. **7**, 649 (1954).
[21] S. Blanes, F. Casas, J. Oteo, and J. Ros, Phys. Rep. **470**, 151 (2009).
[22] H. Batelaan, Contemp. Phys. **41**, 369 (2000).
[23] D. L. Freimund and H. Batelaan, Phys. Rev. Lett. **89**, 283602 (2002).
[24] H. Batelaan, Rev. Mod. Phys. **79**, 929 (2007).
[25] S. Ahrens, *Investigation of the Kapitza-Dirac effect in the relativistic regime*, Ph.D. thesis, Ruprecht-Karls University Heidelberg (2012), `http://archiv.ub.uni-heidelberg.de/volltextserver/14049/`.
[26] S. McGregor, W. C.-W. Huang, B. A. Shadwick, and H. Batelaan, Phys. Rev. A **92**, 023834 (2015).
[27] D. Y. Ivanov, G. L. Kotkin, and V. G. Serbo, Eur. Phys. J. C **36**, 127 (2004).
[28] M. Boca, V. Dinu, and V. Florescu, Nucl. Instrum. Meth. Phys. Res. B **279**, 12 (2012).
[29] K. Krajewska and J. Z. Kamiński, Phys. Rev. A **90**, 052117 (2014).
[30] P. Sancho, Phys. Rev. A **82**, 033814 (2010).